3D SPH-DEM coupling simulation for the large deformation process of sabo dam under debris-flow impact incorporating the nonlinear elastic-plastic bond model

Zheng HAN[1,2], Wendou XIE[1], Fan YANG[1], Yange LI[1,3*], Changli LI[1], Haohui DING[1], Weidong WANG[1], Ningsheng CHEN[4], Guisheng HU[4], Guangqi CHEN[5]

[1] School of Civil Engineering, Central South University, Changsha 410075, China.

[2] Hunan Provincial Key Laboratory for Disaster Prevention and Mitigation of Rail Transit Engineering Structures, Changsha 410075, China.

[3] The Key Laboratory of Engineering Structures of Heavy Haul Railway, Ministry of Education, Changsha 410075, China.

[4] Key Lab of Mountain Hazards and Surface Processes, Institute of Mountain Hazards and Environment, Chinese Academy of Sciences, Chengdu 610041, China.

[5] Department of Civil Engineering, Kyushu University, Fukuoka, 819-0395, Japan.

Corresponding author: Y. Li (liyange@csu.edu.cn), No.22 Shaoshan South Road, School of Civil Engineering, Central South University, Changsha, Hunan, China. Tel.: +86 18684982076.

Key Points:

- A DEM blocks modeling method based on the relatively fixed particles for sabo dam is introduced.
- A nonlinear elastic-plastic bond model with a pre-defined bond strength degradation coefficient α between DEM blocks is incorporated.
- A simple pier failure case and the 2010 Yohutagawa debris-flow event are used to verify the proposed model.

Abstract

The computational analysis of debris-flow dynamics and its impact on the structure, i.e., sabo dam, is a long-standing problem for hazard prevention. It is a complex problem that involves fluid-solid coupling and large deformation process of sabo dam, for which three-dimensional numerical simulation remains a scientific challenge until now. The smooth particle hydrodynamics (SPH) and discrete element method (DEM) coupling model can enable the numerical simulation for the large deformation failure of sabo dam under debris-flow impact. For this purpose, built upon our previous Herschel-Bulkley-Papanastasiou (HBP) rheology-based 3D SPH model, the impact forces posed by debris-flow particles acting on the sabo dam are obtained. The sabo dam is modeled by a series of particles with relatively fixed positions in order to generate blocks for simulating their large deformation by DEM, wherein a nonlinear elastic-plastic bond model with a pre-defined bond strength degradation coefficient α between DEM blocks is incorporated. To verify the effectiveness of the proposed 3D SPH-DEM numerical coupling model, a simple pier failure case under debris-flow impact is simulated in prior, and the 2010 Yohutagawa debris-flow event, at Amami Oshima Island in Japan is selected as a case study, in which sabo dam with different bond strength degradation coefficients are tested. Results show that the proposed 3D SPH-DEM numerical model well simulates the fluid-solid coupling phenomenon and is able to explore the large deformation of the sabo dam with different strengths under debris-flow impact.

Plain Language Summary

Preventing and mitigating debris flow disasters heavily depend on the understanding of debris flow dynamics and the large deformation failure characteristics of sabo dams, which involve complex fluid-solid coupling effects and remain a scientific challenge. Here, we propose a novel 3D SPH-DEM coupling approach to explore the debris-flow dynamics process and the large deformation failure characteristics of sabo dams. This approach uniquely uses a series of relatively fixed particles to model the DEM blocks of the sabo dam. Additionally, a nonlinear elastic-plastic bond model with a pre-defined bond strength degradation coefficient α between DEM blocks is incorporated to simulate different strength states of the sabo dam. A simple pier failure case and the 2010 Yohutagawa debris-flow event are used for testing in this paper, and the results show that the proposed 3D SPH-DEM coupling model well simulates the fluid-solid coupling phenomenon and is able to explore the large deformation of the sabo dam with different strengths under debris-flow impact.

1 Introduction

Debris flow is a major type of geological disaster in mountainous regions, such fluid-solid flows pose significant risks to human settlements in mountainous areas and cause considerable loss of life and property worldwide each year (Han et al., 2014; Dowling & Santi, 2014; Godt & Coe, 2007). Consequently, the use of tangible structural measures (e.g., sabo dams, check dam structures, and levees) to resist the debris-flow impact has become an easily achievable and commonly used strategy to safeguard human life and property (Mizuyama, 2008; Horiguchi & Richefeu, 2020).

However, the debris-flow incidents breaking through sabo dams at upstream of the gully have continued to be reported in recent years. For example, on August 8, 2010, a catastrophic debris flow in Zhouqu city, China, destroying or damaging approximately 5,500 buildings and

numerous sabo dams (Chen et al., 2019; Tang et al., 2011). Additionally, the torrential rainfall event that occurred in the Hiroshima region, Japan in 2018 resulted in the instant collapse of a masonry sabo dam, injuring over 200 people (Tsuguti et al., 2019).

In general, the fundamental reasons for the large deformation failure of sabo dams under debris-flow impact, causing significant losses, can be explained from two scientific perspectives. Firstly, the enormous impact force posed by the high-speed motion of debris flow exceeds the load-bearing capacity of the sabo dams themselves (Shieh et al., 2008; Canelli et al., 2012; Ishikawa et al., 2018). Secondly, the inevitable temporal deterioration effect during the service life of sabo dams leads to a degradation in strength, which is usually caused by complex internal and external factors, e.g., long-term service, concrete protection layer peeling, and rainwater erosion (Gao et al., 2007; Deng et al., 2008; Wang et al., 2016; Burlion et al., 2005). Therefore, the ways of analyzing the debris-flow impact force and reasonably evaluating the temporal deterioration effect of sabo dams has always been a crucial issue in debris flow disaster mitigation research.

In fact, the outbreak of field debris flow is usually unpredictable, making on-site investigations of the debris flow and sabo dams dangerous and challenging to achieve (Chen et al., 2022; Schaefer et al., 2021; Belli et al., 2021). Therefore, flume experiments became one of major ways for this purpose, wherein many remarkable studies could be referred to (Liu et al., 2019; Song et al., 2017; Armanini et al., 2011). However, the majority of the existing flume experimental studies focused on the measurement of debris-flow impact on the structure, while the internal dynamic responses as well as the large deformation of the structures were rarely and difficult to explored. In this sense, providing a feasible solution to describe the large deformation failure of sabo dams under the debris-flow impact remains a significant scientific challenge.

Numerical simulation methods have become a reasonable and acceptable solution. However, the large deformation failure of sabo dams under the debris-flow impact presents extreme numerical simulation difficulties due to the involvement of complex fluid-solid coupling effects (Hasanpour et al., 2021; Yu et al., 2020). The numerical model for simulating this process must include the following important aspects of information, i.e., accurate description of the complex dynamic behavior of the viscous liquid-phase debris flow and its real-time impact force acting on the sabo dams, as well as the reasonable characterization of the large deformation failure characteristics of the solid-phase sabo dams (Zhu et al., 2021).

Currently, there have been numerous previous studies worth referencing (Ouyang et al., 2015; Pirulli & Pastor, 2012) for numerical simulation of complex dynamic behaviors of the liquid-phase debris flow. These previous studies typically utilized 2D mesh-based numerical methods (e.g., FEM, FDM, and FVM) to solve the debris-flow dynamic characteristics. Although their feasibility has been demonstrated, there is still some debates due to their calculation accuracy being heavily dependent on the grid division (Zhu et al., 2021; Huang & Zhu, 2015; Liang & Zhao, 2019). Besides, the 2D numerical models simplified the debris-flow behavior through depth by using a depth-averaged shallow water assumption, limiting the capacity of the proposed model for simulating debris-flow impact on structure. In recent years, meshfree methods, e.g., the Smoothed Particle Hydrodynamics (SPH) has been proven to have incomparable inherent advantages in simulating the dynamic behaviors of geological materials such as the debris flows and landslides (Han et al., 2019; Huang et al., 2012; Huang & Dai, 2014; Zhu et al., 2018), providing a valuable solution for addressing the abovmenetioned issues.

Moreover, accurately obtaining the debris-flow impact force acting on the sabo dams is a crucial prerequisite for constructing this complex fluid-solid coupling model, as existing researches (Moriguchi et al., 2009; Yu et al., 2020) have shown that the debris-flow impact force is the primary means by which buildings and structures within the affected area are damaged by debris-flow. Many previous studies (Armanini, 1997; Lichtenhahn, 1973; Cui et al., 2015; Hübl et al., 2009; Chen et al., 2006; Tiberghien et al., 2007) have provided various solutions for calculating the debris-flow impact force. However, it is necessary to notice that a consensus on the calculation of debris-flow impact force has not yet been reached, and the empirical simplifications and the difficulty in unifying parameter values are the core of the debate in current research of the debris-flow impact force. For instance, the empirical formula for calculating the debris-flow impact force, initially proposed by Armanini (1997) and Lichtenhahn (1973), can be expressed as follows:

$$P = k\rho_{mu} g h_{mu} \tag{1}$$

where P, ρ_{mu}, h_{mu} are the impact force, density, and flow depth of debris flows, respectively, and k is the empirical coefficient. This type of empirical formula simplifies the debris-flow as a single-phase flow, and the calculated value of impact force is highly dependent on the empirical coefficient k. Due to the randomness of the solid materials (e.g., boulder and pebble) in debris-flow mass during its process, the debris-flow impact force shows a significant spatio-temporal variations. Evidence of this phenomenon has been described in the remarkable experimental study conducted by Iverson et al. (2010). Therefore, it is inappropriate to continue using the empirical formulas based on the indicators such as average density and flow depth to calculate the debris-flow impact force. These issues that need further improvement arise a need for a more precise calculation approach of the debris-flow impact force when constructing the complex fluid-solid coupling model.

Besides, another important and unavoidable task is to ensure that the large deformation failure characteristics of the sabo dams are adequately reflected in the complex fluid-solid coupling numerical models (Zhu et al., 2021). Several previous studies (e.g., Wang et al., 2015; Wang & Li, 2017; Chen et al., 2011; Gao et al., 2011; Jia et al., 2011; Liang & Chen, 2019) have employed the SPH-FEM or CFD-FEM methods to simulate the large deformation failure characteristics of sabo dams under the debris-flow impact, which inspire the following studies. These studies have recorded stress-strain response data of the sabo dams and provided insights into the deformation failure mechanisms of such structures. However, these studies have generally relied on the weakly-coupled static analysis and thus cannot capture the strong fluid-solid coupling effects during the debris-flow impact on the sabo dams that are in the state of the temporal deterioration. Furthermore, the mesh-based FEM analysis method used in these studies is often limited in its ability to describe the large deformation failure characteristics of sabo dams due to the distortion phenomenon of mesh elements (Zhu et al., 2021). This research status has stimulated the subsequent research on how to reasonably consider the large deformation failure characteristics of the sabo dams that are in a state of temporal deterioration in the fluid-solid coupling numerical model.

In this paper, a 3D smoothed particle hydrodynamics (SPH) and discrete element method (DEM) coupling model is incorporated based on the Herschel-Bulkley-Papanastasiou (HBP) rheology model we previously proposed. In the model, the debris-flow impact force acting on the sabo dams is obtained through the fluid-solid interaction contact algorithm. The sabo dam is

innovatively modeled as a series of particles with fixed positions in order to simulate its large deformation by the DEM method, and a nonlinear elastic-plastic bond model with a pre-defined bond strength degradation coefficient α is incorporated between the blocks. To verify the effectiveness of the proposed 3D SPH-DEM numerical coupling model, a simple pier failure case is simulated in prior, and the 2010 Yohutagawa debris-flow event in Japan is tested, where the temporal deterioration effect of the sabo dam is represented by the strength degradation coefficient α with different values. This study will show that how the proposed 3D SPH-DEM coupling model simulates the fluid-solid coupling phenomenon and demonstrate the ability of the proposed model to explore the large deformation failure characteristics of the sabo dams with different strengths under debris-flow impact.

2 Methodologies

2.1 Debris flow simulation using the proposed 3D-HBP-SPH model

As mentioned above, due to the limitations of mesh-based numerical models in simulating the complex dynamic behaviors of the liquid-phase debris flow, we employ the particle-based meshfree numerical model in this paper to simulate the dynamics process of the debris flow. In general, this kind of particle-based model provides a 3D description of the debris-flow dynamic process through discrete particles and approximately solves the Navier-Stokes (N-S) equations in discrete form (Hungr & McDougall, 2009; McDougall & Hungr, 2005), so that a large amount of debris-flow dynamic data can be obtained in detail. Considering the complex rheology of debris-flow mass, here we use our previous three-dimensional SPH model based on the Herschel-Bulkley-Papanastasiou (HBP) rheology (Han et al., 2019, 2021), the so-called 3D-HBP-SPH model, the positive effect of which has been substantiated by the following studies (Huang et al., 2022; Morikawa & Asai, 2022; Yu et al., 2020). We choose HBP rheology in our SPH model because this rheology avoid the numerical divergence in conventional Bingham rheology, and able to overall describe the features of different types of fluids, such as Newtonian type, Bingham type, pseudo-plastic type, and dilatant type. The details of this model could be referred to Han et al. (2019) and Han et al. (2021).

2.2 Fluid-solid interaction contact

It should be noted that in order to ensure the basic accuracy of the simulation in the debris-flow dynamics process, typically about 10^5 to 10^6 SPH particles are discretized, which contain important physical information (such as velocity, position, etc.) that needs to be considered when obtaining the debris-flow impact force. Therefore, how to ensure that these massive amounts of information are fully and reasonably utilized during the fluid-solid interaction contact becomes the key to accurately solving the debris-flow impact force. In this paper, a particle-based DEM method is used for the solid-phase sabo dams, which uses a series of closely distributed particles with relatively fixed positions on the surface and inside to construct the DEM blocks. The advantage of this method is that it can uniformly solve the discretized Navier-Stokes (N-S) momentum equation during the fluid-solid interaction contact, thereby achieving the full utilization and coupling of physical information between the SPH particles and the DEM blocks. Figures 1a-b shows this modeling method and the schematic diagram of the fluid-solid interaction contact. After modeling the sabo dams with the above method, the fluid-solid interaction contact process can be summarized into the following three steps:

2.2.1 Particle search in the domain of the interaction contact

After solving the debris-flow dynamics using the 3D-HBP-SPH numerical scheme, the SPH particles and their associated physical information will be highly associated with the calculation time interval Δt. In a certain time step t, these SPH particles will inevitably come into coupled collision with the sabo dam. Therefore, for a specific constituent particle of the DEM blocks (as shown by the yellow particle in Figures 1a-b), the SPH particles that may come into contact with it can be identified by a specific search, as represented by the following equation,

$$r_{ij} \leq L \tag{2}$$

where r_{ij} is the distance between the SPH particle and the constituent particle of DEM blocks, and L is the search length of the constituent particle of DEM block. This search range with the radius of L is called the fluid-solid interaction contact domain in this paper. It is noteworthy that the magnitude of the fluid-solid interaction contact domain is closely correlated with the particle smooth length h, in the event that the value of L is too diminutive, there will be inadequate fluid particles interacting with the constituent particles, thereby resulting in divergent computational outcomes. Conversely, if the value of L is too exorbitant, it will significantly augment the computational expenses and result in a squandering of computing resources (Bui et al., 2021; Lian et al., 2021). As such, according to the general empirical rule, L is conventionally set between the range of $1.2\sim2.0h$. In pursuit of balancing computational precision and expenses, L is set to $2h$ in this paper.

2.2.2 Calculation of the fluid-solid interacting force

When the SPH particles enter the fluid-solid interaction contact domain and its associated physical information is captured by the search, the interaction between the SPH particle and the DEM blocks begins. In this process, the numerical acceleration of each specific constituent particle of the DEM blocks is first solved, and then the Newton's second law is used to solve the resultant force acting on the entire DEM blocks. The calculation formula are as follows,

$$\frac{d\boldsymbol{v}_b^{\alpha}}{dt} = \sum_{j=1}^{N} m_j \left(\frac{p_b + p_j}{\rho_b . \rho_j} + \Pi_{bj} \right) \nabla_b \boldsymbol{W}_{bj} + \boldsymbol{g} \tag{3}$$

$$\boldsymbol{F_{fb}} = M_i \sum_{b=1}^{M} \frac{d\boldsymbol{v}_b^{\alpha}}{dt} \tag{4}$$

where $\frac{d\boldsymbol{v}_b^{\alpha}}{dt}$ represents the numerical acceleration of the constituent particle of the DEM blocks caused by the SPH particles, N is the number of SPH particles in the fluid-solid interaction contact domain, m_j is the mass of each SPH particle, ρ_b, ρ_j, p_b, p_j represent the density and pressure of the constituent particle and the SPH particle, respectively. Π_{bj} represents the artificial viscosity term, $\nabla_b \boldsymbol{W}_{bj}$ is the gradient of the kernel function, $\boldsymbol{g}$ is the gravity term. M_i is the total mass of the DEM blocks, and $\boldsymbol{F_{fb}}$ represent the resultant force acting on the entire DEM blocks due to the SPH particles. It is essential to state that according to the principle of action and reaction, the force exerted by the SPH particles on the DEM blocks will be equal and opposite to the force exerted by the DEM blocks on the SPH particles. Therefore, this fluid-solid interacting force will be inserted into the debris-flow Navier-Stokes momentum equation in turn to control the debris-flow dynamic process during the next time step.

2.2.3 Update of the calculation system

Analogous to other explicit fluid dynamics methodologies, to ensure the continuous acquisition and updating of physical quantities for the ensuing time step, the time integration scheme must be expeditiously executed upon completing all calculation procedures in the preceding time step. Therefore, a calculation system update procedure will be performed here to advance the simulation. In this process, the time step is controlled by the Courant-Friedrichs-Lewy (CFL) condition, which aims to ensure the stability of the explicit time integration scheme. The calculation formula for the variable time step is as follows:

$$\Delta t = C_{CFL} * min(\Delta t_f, \Delta t_{cv}) \tag{5}$$

$$\Delta t_f = min_i(\sqrt{\frac{h}{|f_i|}}) \tag{6}$$

$$\Delta t_{cv} = min_i(\frac{h}{c_0 + max_j \left|\frac{v_{ij} r_{ij}}{r_{ij}^2}\right|}) \tag{7}$$

where Δt represents the new time step, Δt_f is the time step determined by the unit mass force, and Δt_{cv} is the time step determined by the viscous diffusion term. C_{CFL} is the Courant number, a constant of the order of 10^{-1} (Canelas et al., 2016). $|f_i|$ is the force per unit mass, and c_0 is the numerical sound velocity. v_{ij} and r_{ij} represent the velocity difference and coordinate vector between particle i and j, respectively. Subsequently, the symplectic time integration scheme is adopted. The above steps are iteratively executed until the calculation time step reaches the termination time, and then the simulation ends.

2.3 The nonlinear elastic-plastic bond model

In addition, a nonlinear elastic-plastic bond model is introduced to accurately characterize the large deformation failure characteristics of sabo dams that are in the state of the temporal deterioration. The normal and tangential collision constraint forces between the constituent particle constraint pairs of the DEM blocks can be represented by a set of normal and tangential springs in this model, as shown in Figure 1c. Furthermore, a bonding block is added to the constituent particles of the DEM blocks to simulate the strength degradation phenomenon of the sabo dams, which is abstractly shown in Figure 1d. With the addition of the bonding block, the force state of the DEM blocks is changed and can be expressed by the following equations,

$$[\boldsymbol{F}]^T = \left[\boldsymbol{F_{fb}}\right]^T + \left[\boldsymbol{F_{pb}}\right]^T - [\boldsymbol{F_{bb}}]^T \tag{8}$$

$$\left[\boldsymbol{F_{pb}}\right]^T = \left[\boldsymbol{F_{pb}^n}\right]^T + \left[\boldsymbol{F_{pb}^\tau}\right]^T \tag{9}$$

where $\boldsymbol{F}$ represents the total force acting on the DEM blocks of sabo dam, $\boldsymbol{F_{fb}}$, $\boldsymbol{F_{pb}}$ represent the force generated by the debris-flow SPH particles and the collision constraint force between the constituent particles, and $\boldsymbol{F_{bb}}$ is the force allocated to the bonding block. $\boldsymbol{F_{pb}^n}$, $\boldsymbol{F_{pb}^\tau}$ represent the normal and tangential collision constraint forces between the constituent particles, respectively, which can be calculated based on Canelas et al. 2016. In addition, a pre-defined bond strength degradation coefficient α, which is specially designed to calculate the force state of the bonding

block, is incorporated to complete the construction of the nonlinear elastoplastic model, as a result, the force state of the bonding block can be expressed by the following equation,

$$[\boldsymbol{F_{bb}}]^T = \alpha \left[\boldsymbol{F_{pb}}\right]^T \tag{10}$$

Therefore, Equation (8) can be rewritten in the following form,

$$[\boldsymbol{F}]^T = \left[\boldsymbol{F_{fb}}\right]^T + (1-\alpha)\left[\boldsymbol{F_{pb}}\right]^T \tag{11}$$

As demonstrated in Equation (10), coefficient α is employed to coalesce the stresses attributed to the bonding block and the constituent particles in parallel. As per the Equation (9), the stress level borne by the DEM blocks of sabo dam is inversely proportional to coefficient α. A greater value of α corresponds to a smaller stress value shouldered by the DEM blocks of sabo dam, thereby resulting in a more stable configuration of the sabo dam. Conversely, a smaller value of α engenders a higher stress level shouldered by the DEM blocks of sabo dam, rendering the sabo dam more vulnerable to large deformation and failure.

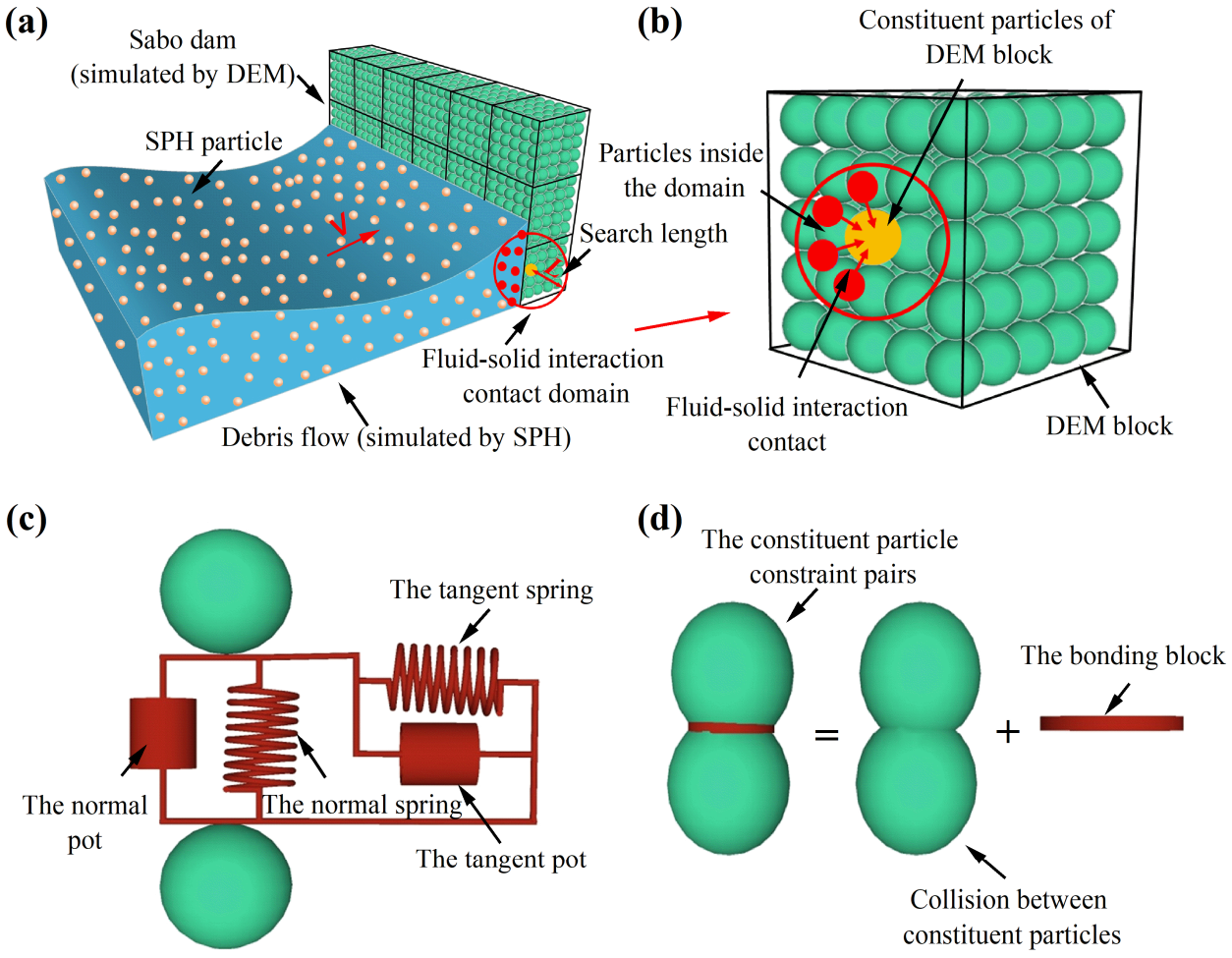

Figure 1. (a) Schematic diagram of the interaction contact between debris-flow and sabo dam. (b) The DEM modeling method for the solid-phase sabo dam. (c) Schematic diagram of the mutual constraint. (d) Schematic diagram of the bonding block.

Subsequently, Newton's equations for rigid body dynamics are used to described the motion characteristics of the DEM blocks,

$$M_i \frac{d\boldsymbol{V}_i}{dt} = \boldsymbol{F} \tag{12}$$

$$\boldsymbol{I}_i \frac{d\boldsymbol{\Omega}_i}{dt} = \boldsymbol{F} \times (\boldsymbol{r_k} - \boldsymbol{R}_i) \tag{13}$$

where $\boldsymbol{V}_i$ and $\boldsymbol{I}_i$ represent its velocity and inertial tensor, respectively. $\boldsymbol{\Omega}_i$ and $\boldsymbol{R}_i$ represent the angular velocity and centre of gravity, respectively.

3 Model test using the simple pier failure case

To verify the effectiveness of the proposed coupling model, a simple pier failure case is simulated in prior. The pier is simplified as a square column with the size of 0.15 × 0.15 × 0.45 m and placed in a computational domain of 5.0 × 0.7 × 0.6 m. The distance between the impacted surface of the pier and the upstream wall is 2.7 m. It is assumed that the size of the debris flow is 1.0 × 0.7 × 0.4 m, and the debris-flow mass is close to the left side wall of the computational domain at the initial time. The schematic diagram of the simple pier failure case is shown in Figure 2a. It is significant to point out that the bonding interface under the temporal deterioration effect between the DEM blocks and the bonding block (also called as the strength degradation type pier) will be simulated first, with the pre-defined bond strength degradation coefficient of 0.4. In this simulation, the positive bonding effect between the DEM blocks is no longer prominent, and the degraded bonding block only bears 40% of the stress level carried by the constituent particles of DEM blocks. The majority of the stress level is borne by the pier, indicating that the pier is more susceptible to large deformation failure. The key simulation parameters under this condition are summarized in Table 1.

Table 1. Key simulation parameters of the simple pier failure case

Parameters	Notation	Unit	Value
Density	ρ	kg/m^3	1600
Dynamic viscosity	μ	Pa·s	0.01
Cohesion	coh	Pa	0
Frictional angle	Φ	°	40
Key coefficients of HBP model	m	/	10
Key coefficients of HBP model	n	/	1.50
Particle spacing	Dp	m	0.0125
Smooth length	l_s	m	0.19364
The artificial viscosity coefficient	$\alpha_{\mathrm{II}}, \beta_{\mathrm{II}}$	/	0.1
State constant	γ	/	7
Total fluid particles	N_{pf}	n	140800
Total block particles	N_{kf}	n	6591
Total boundary particles	N_{pb}	n	66633
The Young's modulus of the pier	E	N/m^2	8×10^9
The Poisson's ratio of the pier	V	/	0.35
The bond strength degradation coefficient	α	/	0.4
Simulation duration	T	s	2.0

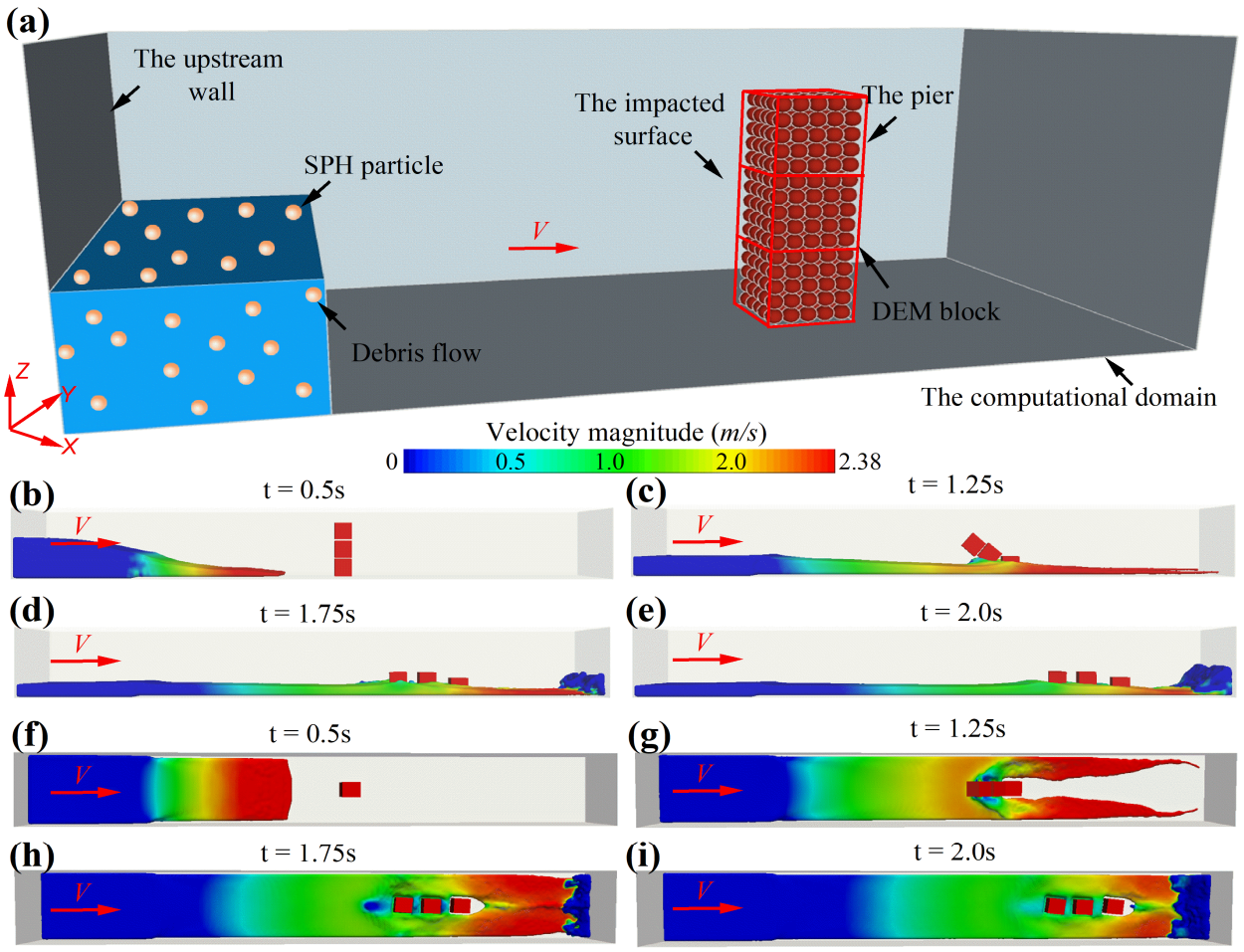

Figure 2. (a) Schematic diagram of the simple pier failure case. The debris-flow velocity distribution graphs of this case (lateral view) at (b) t = 0.5 s, (c) t = 1.25 s, (d) t = 1.75 s, (e) t = 2.0 s. The debris-flow velocity distribution graphs of this case (top-down view) at (f) t = 0.5 s, (g) t = 1.25 s, (h) t = 1.75 s, (i) t = 2.0 s.

Figures 2b-i shows the debris-flow velocity distribution and the large deformation failure of the strength degradation type pier in different instants under the above simulation conditions. It can be observed from the Figure 2 that the maximum velocity of the dam-breaking debris flow reaches 2.38 m/s, and the maximum displacement and average velocity of the pier are calculated by analyzing the output results of the pier, which are 1.35 m and 1.38 m/s, respectively. Besides, some representative failure moments of the strength degradation type pier are selected and presented in Figure 3. As demonstrated in Figure 3, at t = 0.64 s , the debris-flow mass initiates collision with the pier blocks. Furthermore, a result was also inferred from the output results of the pier, indicating that the debris-flow mass caused a large deformation failure of approximately 15 cm to the bottom blocks of the pier within the following 0.4s. In a word, in the aforementioned test, the debris-flow dynamic process and the large deformation failure characteristics of the strength degradation type pier were effectively simulated and demonstrated.

In addition to simulating the large deformation failure of the strength degradation type pier, undamaged DEM blocks of the pier with high strength under the debris-flow impact could be also effectively simulated. This operation ensures a comprehensive validation for the proposed

3D SPH-DEM coupling model. Figure. 4 shows the resulting displacement of the DEM blocks of the high strength type pier subjected to debris-flow impact, where the bond strength degradation coefficient α is predefined to $\alpha = 1.0$ in this situation. In this simulation, the positive bonding effect between the DEM blocks is prominent, and the bonding block shares the stress level carried by the constituent particles of the DEM blocks equally. The pier will bear less stress, indicating a more stable structure system.

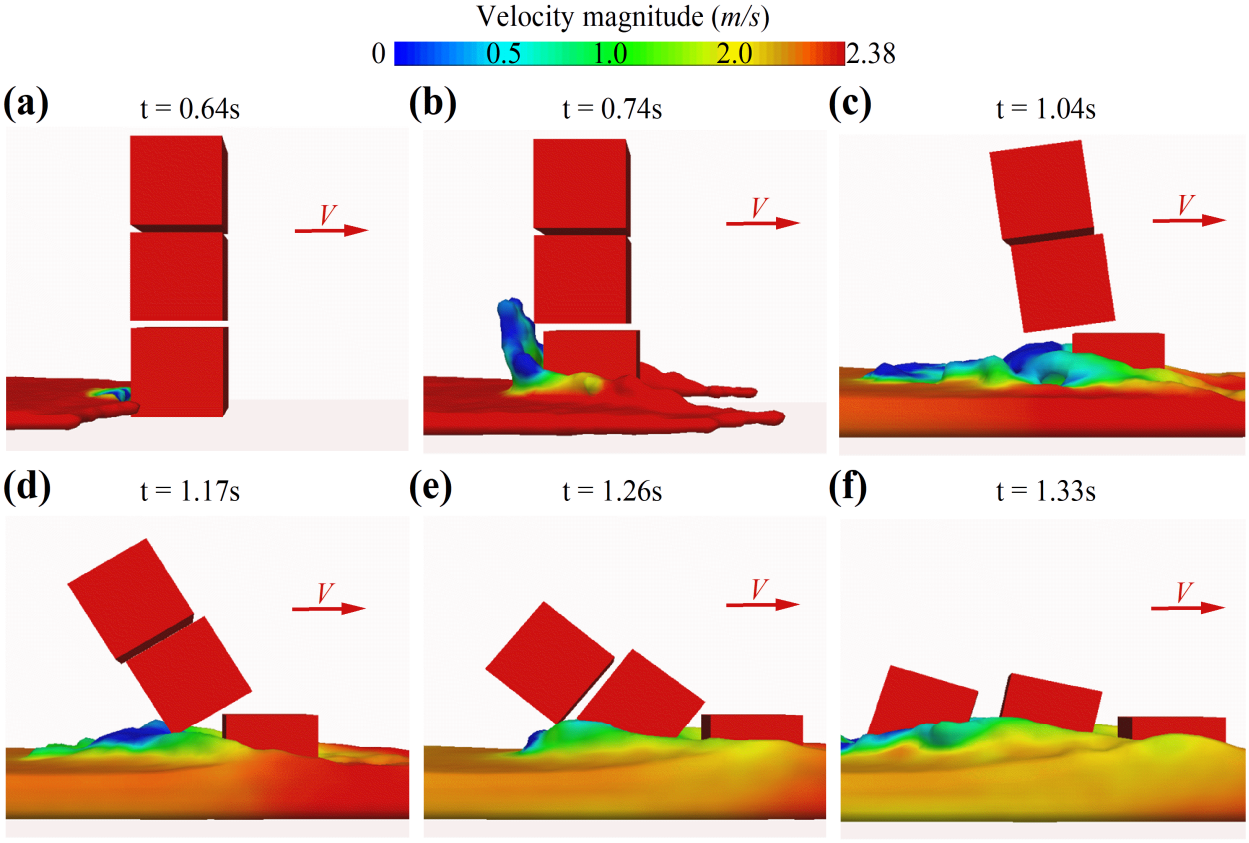

Figure 3. Some representative failure moments of the DEM blocks of the strength degradation type pier. (a) $t = 0.64$ s, (b) $t = 0.74$ s, (c) $t = 1.04$ s, (d) $t = 1.17$ s, (e) $t = 1.26$ s, (f) $t = 1.33$ s.

To be specific, Figures 4a-d present some schematic diagrams at representative instants, while Figures 4e-g depict displacement, velocity, and acceleration comparison graphs of the pier with two strength conditions. From the representative schematic diagrams in Figures 4a-d, it can be observed that the integrity of the high strength type pier remains relatively intact, and significant large deformation failure does not occur. Only a certain degree of sliding occurs in the overall position of the high strength type pier, which is attributed to the lack of frictional contact at the bottom of the pier. This phenomenon verifies the feasibility of simulating large deformation of the pier with different strength levels by changing the pre-defined bond strength degradation coefficient α. Furthermore, the displacement, velocity, and acceleration comparison graphs of the pier with two strength conditions in Figures 4e-g under the same simulation parameters reveal that the strength degradation type pier exhibits higher values than the ones with high strength, which agrees well with the actual situation. In summary, the test of the simple pier failure case demonstrates that the effectiveness of the proposed 3D SPH-DEM coupling model, which is capable of not only simulating the large deformation failure of the strength degradation

type structures, but also simulating the deformation of structures with high strength after being impacted by the debris-flow.

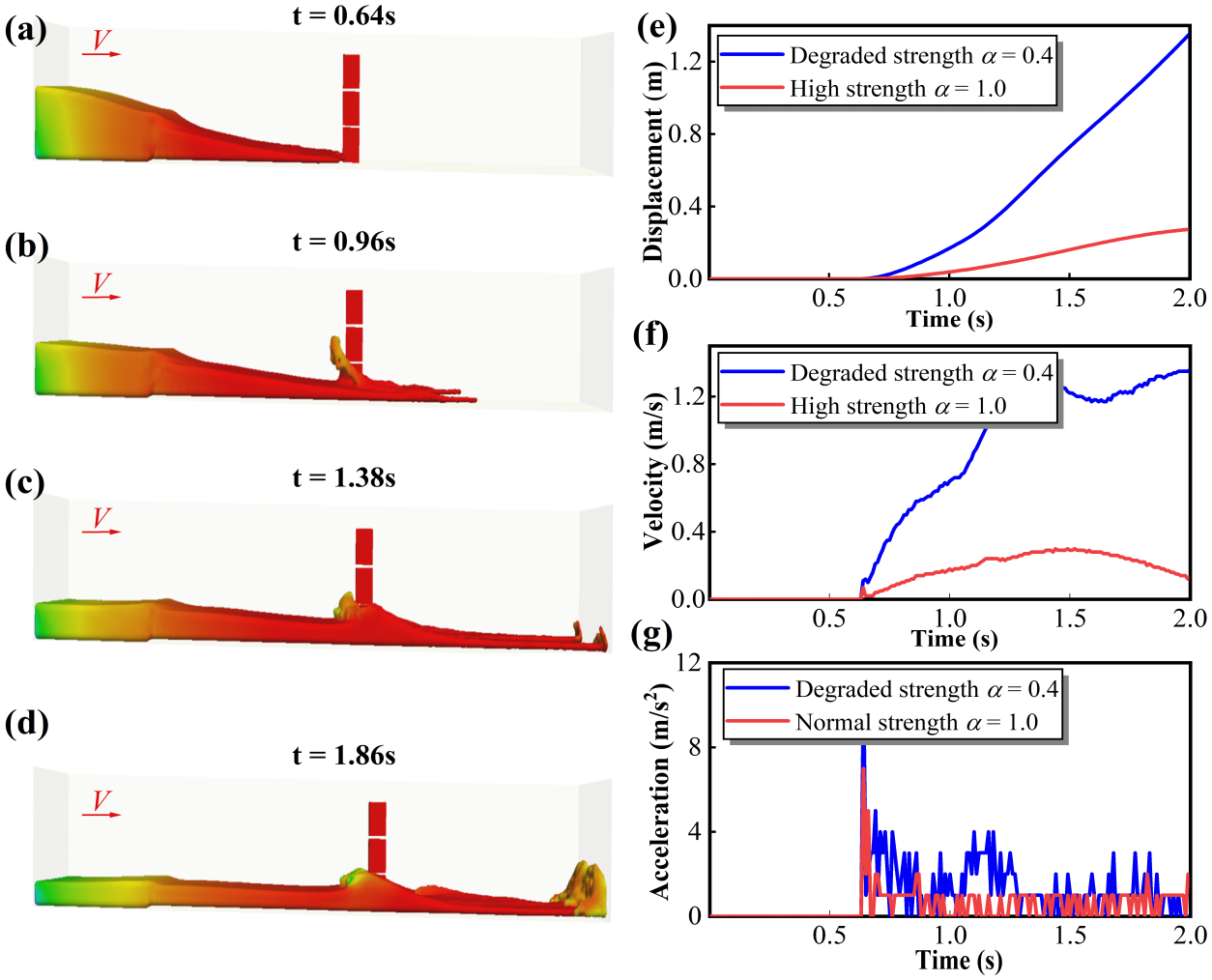

Figure 4. Some representative moments of the pier with high strength. (a) t = 0.64 s, (b) t = 0.96 s, (c) t = 1.38 s, (d) t = 1.86 s. (e) The displacement comparison graph with two strength conditions. (f) The velocity comparison graph with two strength conditions. (g) The acceleration comparison graph with two strength conditions.

4 Case study: The 2010 Yohutagawa debris-flow event

The model test using the simple pier failure case has inspired us to simulate more actual debris-flow events to test the practicality of our proposed 3D SPH-DEM coupling model. Here, the 2010 Yohutagawa debris-flow has been selected as a case study.The 2010 Yohutagawa debris-flow event occurred on Amami Oshima Island in southwest Japan. The area of the catchment is 0.24 km^2, with elevations ranging from 20 m to 250 m, as illustrated in Figure 5a. According to the post-disaster investigation, the event was triggered by intense rainfall accompanying Typhoon Megi on Oct. 20, 2010. Although the majority of the debris mass was intercepted by the sabo dam at the outlet of the channel, some overflowed the dam, resulting in damage to two buildings on the alluvial fan. For further information on this event, please refer to our previous research (Han et al., 2015a).

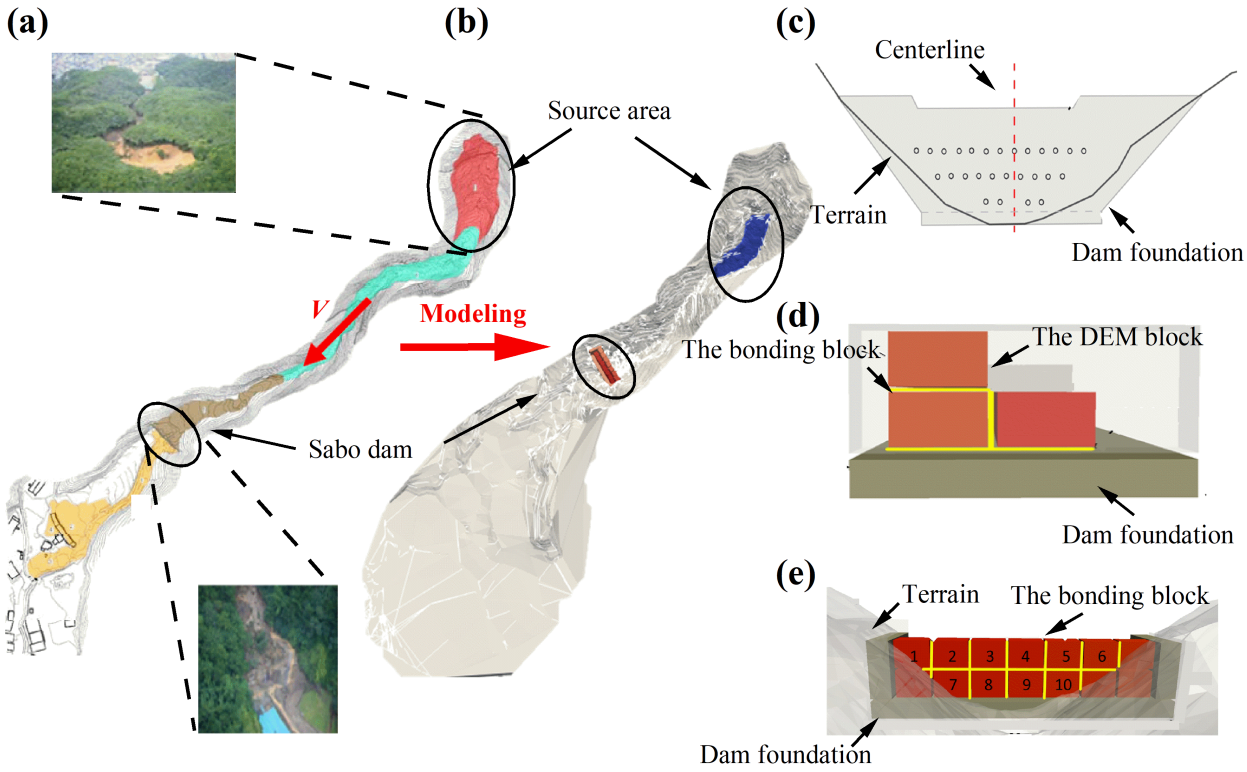

Figure 5. (a) The 2010 Yohutagawa debris flow event in Japan. (b) The model of this event. (c). The plan view of the sabo dam. (d) The side view of the sabo dam. (e) The cross-section of the sabo dam.

4.1 Simulation configuration

At the initial stage of model development, a set of digital elevation data interpreted from a 1:2000 countour map from the Geological Survey of Japan (GSJ) was employed to create the topograph of the gully. As shown in Figure 5b, the initiation debris-flow source area and the position of the sabo dam were embedded in the terrain based on the actual conditions. Additionally, Figures 5c-d illustrate the plan view, side view, and cross-section of the sabo dam in the model, respectively. The key parameters used are summarized in Table 2. It is crucial to highlight that it is similar to the simple pier failure test, the bond strength degradation coefficient α is predefined as 0.4 in the initial simulation to simulate the strength degradation type sabo dam that is in the state of the temporal deterioration.

4.2 Simulation results of the Yohutagawa debris flow event

The simulation results of the 2010 Yohutagawa debris flow event are presented from a global perspective in Figures 6a-h. It can be observed that on the virtualized model terrain, the entire dynamic process of the debris-flow mass from its initiation state to the collision with the sabo dam is fully displayed. Furthermore, the details of the interaction contact between the debris-flow and the sabo dam are specifically presented in Figures 6i-p, providing a prerequisite and guarantee for obtaining detailed information on the large deformation failure characteristics of the sabo dam. According to the Figures 6i-p, at t = 17.5 s, the debris-flow mass begins to contact the sabo dam and mainly impacts the bottom of the sabo dam. By the simulation time of 20 seconds, the sabo dam gradually experiences significant deformation failure. The post-analysis

of the output calculation results for the sabo dam revealed that it experienced a maximum deformation of approximately 2.98 m. At the end of the simulation (t = 50 s), the sabo dam has been completely destroyed, and parts of the debris-flow mass is trapped behind the remaining sabo-dam bodies.

Table 2. Key simulation parameters of the 2010 Yohutagawa debris flow event

Parameters	Notation	Unit	Value
Density *	ρ	kg/m^3	1650
Cohesion *	coh	Pa	0
Frictional angle *	φ	°	28
Dynamic viscosity	μ	Pa·s	1.255
Key coefficients of HBP model **	m	/	100
Key coefficients of HBP model **	n	/	1.0
Particle spacing	dp	m	0.8
Smooth length***	l_s	m	1.3856
The artificial viscosity coefficient	$\alpha_{\mathrm{II}}, \beta_{\mathrm{II}}$	/	0.1
State constant	γ	/	7
Total fluid particles	N_{pf}	n	39949
Total block particles	N_{kf}	n	52393
Total boundary particles	N_{pb}	n	939941
The Young's modulus of the sabo dam	E	N/m^2	8×10^9
The Poisson's ratio of the sabo dam	v	/	0.35
The bond strength degradation coefficient	α	/	0.4
Simulation duration	T	s	50.0

* Based on the field investigation and laboratory experiment results of this debris-flow event.

** Based on the numerical simulation experience.

*** The smooth length in 3-D can be calculated $l_s = \epsilon\sqrt{(d_{px})^2 + (d_{py})^2 + (d_{pz})^2}$. The coefficient ϵ is determined as 1.0 in the simulation. The d_{px}, d_{py} and d_{pz} denote the SPH particle distance in X, Y and Z direction, respectively.

Analyzing the simulation results, a special DEM block of the sabo dam (named as the Block-2) are observed, as shown in Figure 7a. During the initial contact between the debris-flow and the sabo dam, the maximum deformation failure occurred in this block. Particularly, its maximum displacement, velocity, and acceleration reached as high as 46.1 m, 17.73 m/s, and 6.85 m/s^2, respectively. The motion of this sperated block lasted for 6 seconds during the entire 50-second simulation process. Subsequently, due to the continuous dissipation of the debris-flow kinetic energy, this block no longer moved forward. More information on the motion of this critical block is concentratedly shown in Figures 7b-d. Besides, a seemingly universal law was once again discovered by analyzing Figure 6 and Figure 7, which suggests that the DEM blocks of sabo dams that experience the most significant deformation failure are always concentrated in the middle section of the sabo dam (as shown in Figure 7a, Block-2 is located in the middle of the sabo dam). This phenomenon was also observed and studied by Han et al. (2015b). The reason for this phenomenon can be explained by the debris-flow velocity distribution properties, which have already reached a consensus in the academic discipline, that is, the velocity values in the middle section of the debris-flow velocity profile are significantly higher than those on the

410 sidewalls, thus will cause more significant impact damage to the middle section of the sabo dam.

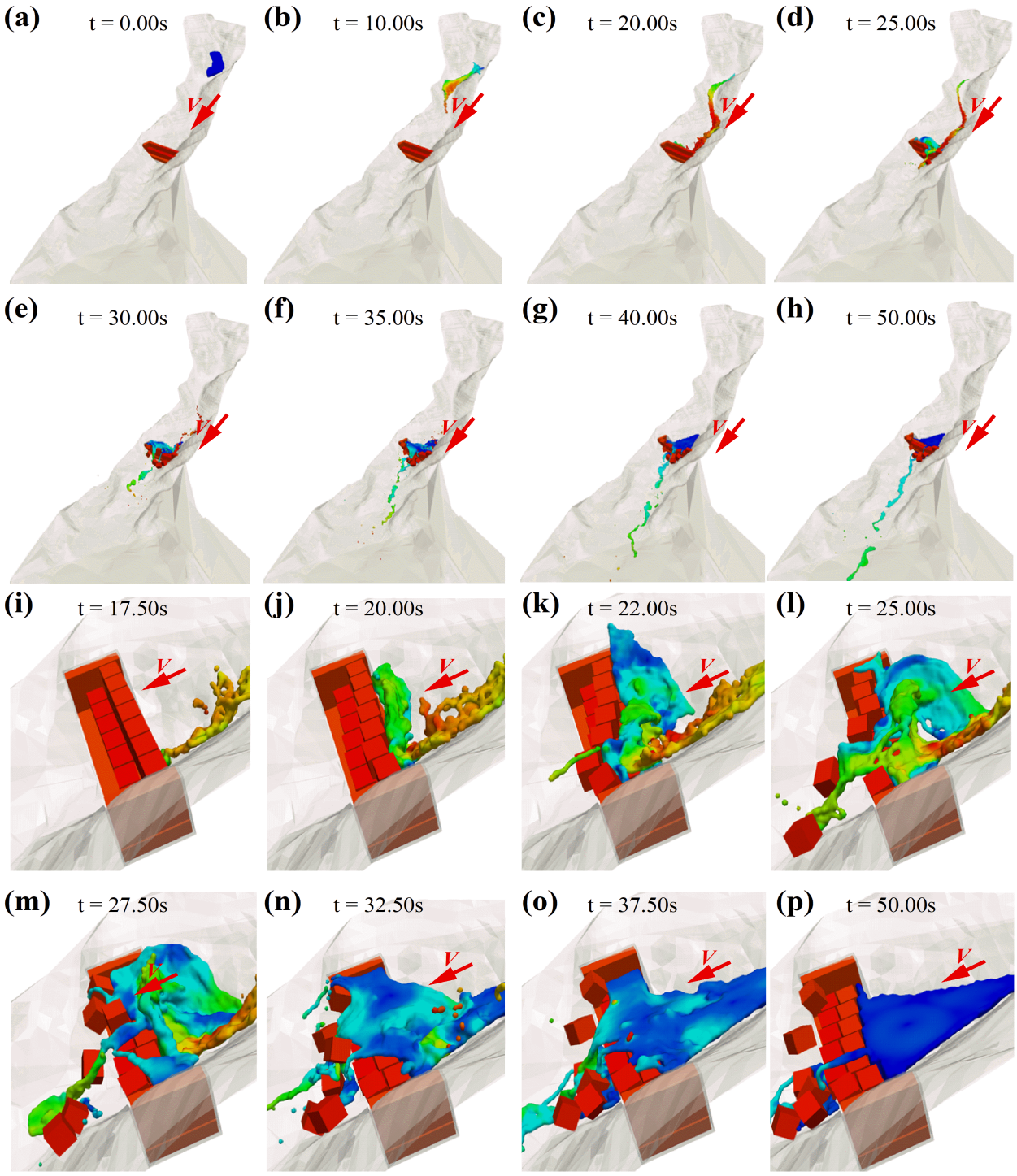

411

412 **Figure 6**. The global views of the simulation results of the 2010 Yohutagawa debris-flow event
413 at (a) t = 0.00 s, (b) t = 10.00 s, (c) t = 20.00 s, (d) t = 25.00 s, (e) t = 30.00 s, (f) t = 35.00 s, (g) t
414 = 40.00 s, (h) t = 50.00 s. The detail views of the interaction contact between debris-flow and the
415 strength degradation type sabo dam at (i) t = 17.50 s, (j) t = 20.00 s, (k) t = 22.00 s, (l) t = 25.00 s,
416 (m) t = 27.50 s, (n) t = 32.50 s, (o) t = 37.50 s, (p) t = 50.00 s.

This phenomenon inspired our academic suggestion to the departments responsible for mitigating the debris-flow disasters. Namely, when constructing preventive sabo dams in the areas where debris flow disasters may occur, particular attention should be paid to the structural strength of the middle section of the sabo dam to enhance the disaster prevention capability.

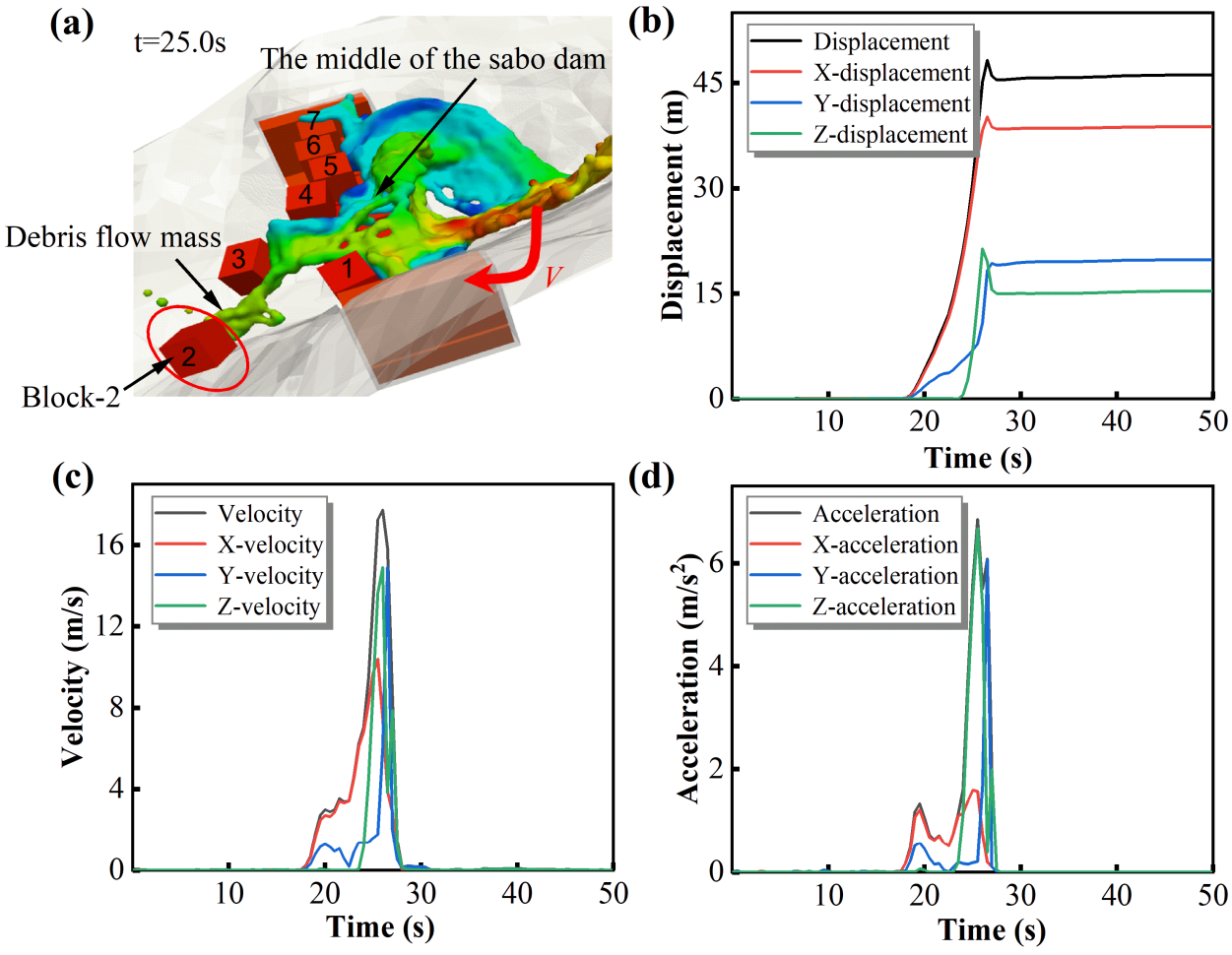

Figure 7. (a) The special block-2 and its failure characteristics. (b) The displacement diagram of the block-2. (c). The velocity diagram of the block-2. (d) The acceleration diagram of the block-2.

4.3 Analysis of the high-strength sabo dam

In Subsection 4.2, the large deformation failure characteristics of the strength degradation type sabo dams were well simulated in the 2010 Yohutagawa debris-flow event. However, the occurrence of debris-flow disasters is stochastic, and there is still a possibility of the high-strength sabo dams, which have just been completed and have not yet experienced the temporal degradation effect, being impacted by the debris flow. Therefore, this situation is fully considered and simulated in this subsection.

The simulation results of this situation are presented in detail in Figure 8. It is to be emphasized that the bond strength degradation coefficient α is predefined as 1.0 to simulate the high strength typr sabo dam in this situation. From the analysis of Figure 8, it can be observed that compared

with the sabo dam with a bond strength degradation coefficient of 0.4, the deformation of the high strength type sabo dam is significantly reduced, and the integrity of the dam is well preserved during the entire debris-flow process. Moreover, its disaster mitigation effect is greatly improved. This once again demonstrates the feasibility of simulating deformation characteristics of sabo dams with different strength levels by changing the bond strength degradation coefficient value in the proposed 3D SPH-DEM model. The information presented in Figure 8 also reveals a noteworthy phenomenon, that the debris-flow disaster mitigation capability of the high strength type sabo dams depends more on their capacity. As shown in Figure 8g, although the high strength type sabo dam has a better retention effect on the debris flow, the possibility of the debris-flow overflowing and impacting downstream buildings cannot be ruled out due to limited capacity of the sabo dam. Therefore, the debris-flow disaster mitigation department should not only pay attention to the strength grade of the sabo dam, but also fully consider and analyze its capacity in some cases.

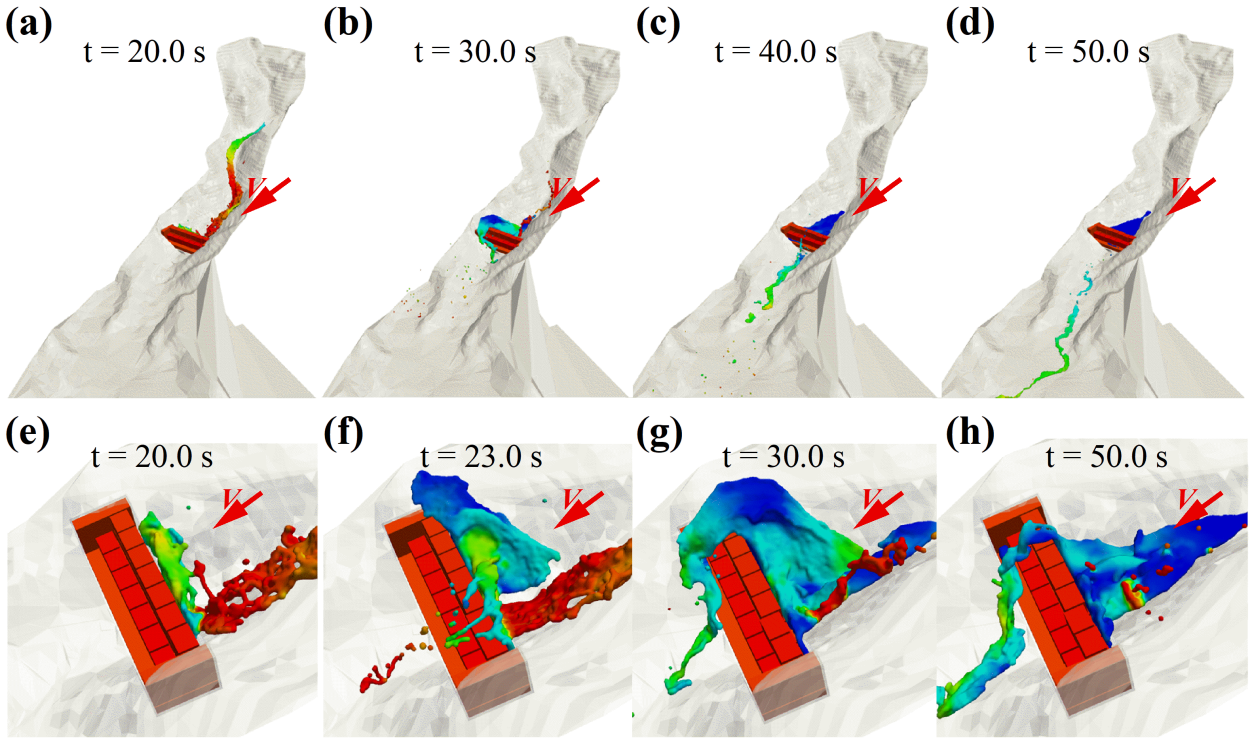

Figure 8. The global views of the simulation results of the high strength type sabo dam at (a) t = 20.0 s, (b) t = 30.0 s, (c) t = 40.0 s, (d) t = 50.0 s. The detail views of the interaction contact between debris-flow and the high strength type sabo dam at (e) t = 20.0 s, (f) t = 23.0 s, (g) t = 30.0 s, (h) t = 50.0 s.

5 Discussion

5.1 An analysis for the bond strength degradation coefficient α

As demonstrated in Sections 3 and Sections 4, the proposed 3D SPH-DEM coupling model possesses unique capabilities for analyzing the large deformation and failure characteristics of sabo dams under debris-flow impact. However, a noteworthy question remains in the model. Specifically, the rationality of simulating different strength levels of sabo dams by artificially

predefining the bond strength degradation coefficient α needs to be scrutinized. It is well-known that due to the special working environment of sabo dams, their strength is subject to unavoidable long-term behavior or temporal deterioration effects (Burlion et al., 2005; Deng et al., 2008). For example, Gao et al. (2007) pointed out that the strength of sabo dams is closely related to the fluidity and density changes of their internal material components, and the entrance of water and other harmful substances through cracks can significantly reduce the service life and durability of sabo dams. Wang et al. (2016) also indicated that the strength of sabo dams will be affected by different load rates. These external factors, which severely affect the strength of sabo dams, exhibit highly spatio-temporal stochasticity and make it difficult to quantitatively and objectively simulate them through a unified mathematical model. Therefore, it exacerbates the difficulty of accurately defining the strength of sabo dams in the proposed 3D SPH-DEM coupling model. It is evident that the next research focus should be integrating the value selection of the bond strength degradation coefficient α with the actual state of sabo dams to reasonably determine its value in the proposed model. This can significantly enhance the persuasiveness of the proposed model. However, at present, the compromise adopted by this paper for the bond strength degradation coefficient α still aligns with the initial intention and positioning of the study as a preliminary investigation.

5.2 Mass and momentum growth of debris-flow

Several studies have substantiated that the rainfall events and entrainment process can enhance the magnitude of debris flow (e.g., Lverson et al., 2011; Stoffer et al., 2014), mainly manifested in the supplement of liquid-phase substances by rainfall events and the supplement of solid-phase substances by entrainment process, which can be summarized in the mechanical perspective as the mass growth and momentum growth of debris flow. In this sense, both important aspects should be fully taken into account in the three-dimensional, SPH-based model of debris flow dynamics. However, this will significantly increase the development difficulty of the proposed model and greatly increase the computational cost. Because the addition of new SPH particles to the computational model will alter the storage and access methods that were designed for existing SPH particles in the computer memory, it will be the most time-consuming part in simulating large-scale cases (Yan et al., 2009), such as those with a particle number of 10^5 to 10^6. In this study, to simulate the 2010 Yohutagawa debris flow event without a hitch, a compromise has been made by ignoring the additional terms caused by the rainfall events and entrainment process in the mass conservation equation and momentum conservation equation. The effects of this limitation on the accuracy of the proposed 3D SPH-DEM model require further investigation.

5.3 Threshold analysis of coefficient α for the occurrence of large deformation failure

As shown in Section 4, the successful simulation of the 2010 Yohutagawa debris-flow event demonstrates the comprehensive performance of the proposed 3D SPH-DEM coupling model. However, it should be noted that an interesting problem closely related to the Yohutagawa debris-flow event continues to attract our research, namely, the threshold value of the bond strength degradation coefficient α when the sabo dam undergoes large deformation failure. Clearly, this threshold value should be between 0.4 to 1.0. Nevertheless, since the interval [0.4, 1.0] contains infinitely many rational numbers, it is not practical to obtain an accurate value for the threshold. Therefore, some pre-defined values for the bond strength degradation coefficient

α, such as 0.5, 0.6, 0.7, 0.8, and 0.9, were used for simulation. The simulation results are shown in Figure 9.

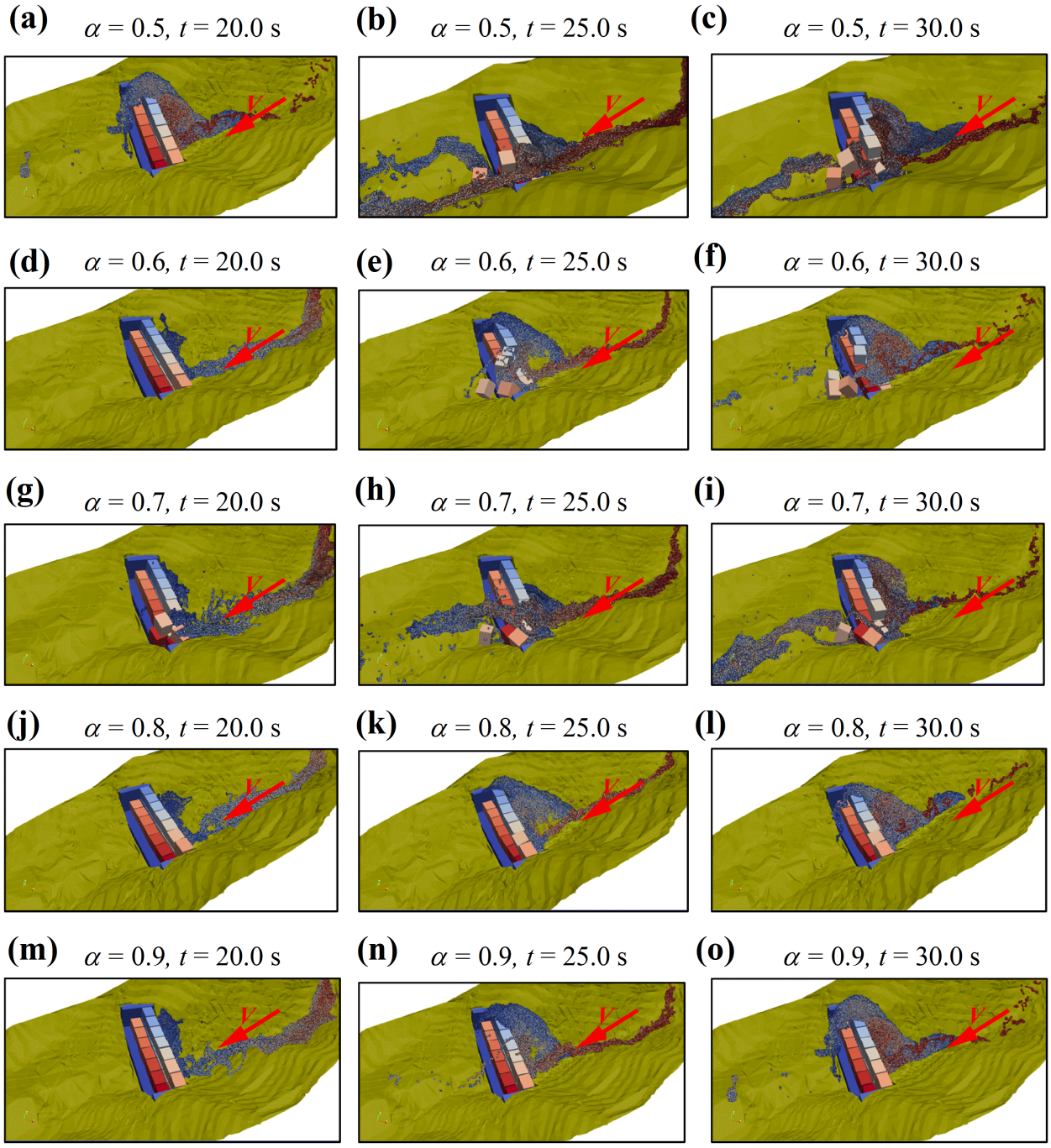

Figure 9. Large deformation graphs of sabo dam under different bond strength degradation coefficients. (a) α = 0.5, t = 20.0 s, (b) α = 0.5, t = 25.0 s, (c) α = 0.5, t = 30.0 s, (d) α = 0.6, t = 20.0 s, (e) α = 0.6, t = 25.0 s, (f) α = 0.6, t = 30.0 s, (g) α = 0.7, t = 20.0 s, (h) α = 0.7, t = 25.0 s, (i) α = 0.7, t = 30.0 s, (g) α = 0.8, t = 20.0 s, (k) α = 0.8, t = 25.0 s, (l) α = 0.8, t = 30.0 s, (m) α = 0.9, t = 20.0 s, (n) α = 0.9, t = 25.0 s, (o) α = 0.9, t = 30.0 s.

From Figure 9, it can be observed that the large deformation of the sabo dam varies significantly under different bond strength degradation coefficients. A gradually mitigated failure of the sabo dam is observed from 0.5, 0.6 to 0.7. When α is predefined as greater than or equal to 0.8, a significant large deformation is difficult to capture, and only a small deformation is noticed at α = 0.8 and t = 30 s. When α = 0.9, the deformation of the sabo dam is barely noticeable. Therefore, it is reasonable to believe that the threshold of the bond strength degradation coefficient in the Yohutagawa debris-flow event is between [0.8, 0.9]. The acquisition of this threshold value provides an important reference for future simulation of similar debris-flow events.

6 Conclusion

This paper proposes a new 3D SPH-DEM coupling model to analyze the large deformation failure characteristics of sabo dams under the debris-flow impact. The 3D-HBP-SPH numerical model, which was previously developed, is used to participate in constructing our coupled model and simulate the debris-flow dynamic process, and the debris-flow impact force is obtained in detail through the fluid-solid contact algorithm.

In order to characterize the sabo dam, we innovatively construct DEM blocks of the sabo dam by a series of particles with relatively fixed positions, and introduce a nonlinear elastic-plastic bond model with a pre-defined bond strength degradation coefficient α between the DEM blocks, and this bond model can simulate sabo dam with different strengths by predefining the bond strength degradation coefficient α.

We test the proposed 3D SPH-DEM coupling model by simulating the simple pier failure case and the 2010 Yohutagawa debris flow event, and the results show that the proposed 3D SPH-DEM coupled model well simulates the fluid-solid coupling phenomenon and is able to explore the large deformation and failure characteristics of the sabo dam with different strengths under the debris-flow impact.

Finally, some discussions related to the limitations of the model and the threshold of bond strength degradation coefficient are presented. Efforts to address these limitations will constitute future research to improve the proposed 3D SPH-DEM coupling model. In addition, the acquisition of the threshold of the bond strength degradation coefficient in the Yohutagawa debris-flow event also provides a scientific reference for future simulation of similar debris-flow events.

Acknowledgments

This study was financially supported by the National Natural Science Foundation of China (Grant No. 52078493); the Natural Science Foundation of Hunan Province (Grant No. 2022JJ30700); the Natural Science Foundation for Excellent Young Scholars of Hunan (Grant No. 2021JJ20057); the Innovation Provincial Program of Hunan Province (Grant No. 2020RC3002). These financial supports are gratefully acknowledged.

Author contributions

Z.H. directed the program. W.D.X. and F.Y performed all the simulations. Z.H., W.D.X and Y.G.L. wrote the manuscript with the help and advice from W.D.W. and G.Q.C. N.S.C. and

G.S.H. reviewed and edited the manuscript. All authors participated in data analysis, discussed the results and co-edited the manuscript.

Competing interests

The authors declare no competing interests.

Data availability

The code in this study is compiled on the *Visual Studio 2015* platform. The SPH implementation code referenced in this study can be obtained at *https://github.com/DualSPHysics.* More detailed information about the 2010 Yohutagawa debris flow event replicated in this study can be obtained at *https://doi.org/10.1016/j.enggeo.2015.02.009.*

References

Armanini, A. (1997), On the dynamic impact of debris flows. *Recent Developments on Debris Flows. In: Armanini A, Michiue M (eds) Lecture notes in earth sciences.* Springer, Berlin, pp. 208-224.

Armanini, A. R. O. N. N. E., Larcher, M., & Odorizzi, M. (2011), Dynamic impact of a debris flow against a vertical wall. *Italian Journal of Engineering Geology and Environment*, 1. *https://doi.org/10.4408/IJEGE.2011-03.B-113*

Belli, G., Marchetti, E., Walter, F., McArdell, B., Chmiel, M., & Wenner, M. (2021), Investigating infrasound sources within Illgraben debris-flows. *In: EGU General Assembly Conference Abstracts.* pp. EGU21-1226. *https://doi.org/10.5194/egusphere-egu21-1226*

Bui, H. H., & Nguyen, G. D. (2021), Smoothed particle hydrodynamics (SPH) and its applications in geomechanics: From solid fracture to granular behaviour and multiphase flows in porous media. *Computers and Geotechnics*, 138, 104315. *https://doi.org/10.1016/j.compgeo.2021.104315*

Burlion, N., Bourgeois, F., & Shao, J. F. (2005), Effects of desiccation on mechanical behaviour of concrete. *Cement and concrete composites*, 27(3), 367-379. *https://doi.org/10.1016/j.cemconcomp.2004.05.004*

Canelas, R. B., Crespo, A. J., Domínguez, J. M., Ferreira, R. M., & Gómez-Gesteira, M. (2016), SPH–DCDEM model for arbitrary geometries in free surface solid–fluid flows. *Computer Physics Communications*, 202, 131-140. *https://doi.org/10.1016/j.cpc.2016.01.006*

Canelli, L., Ferrero, A. M., Migliazza, M., & Segalini, A. (2012), Debris flow risk mitigation by the means of rigid and flexible barriers–experimental tests and impact analysis. *Natural Hazards and Earth System Sciences*, 12(5), 1693-1699. *https://doi.org/10.5194/nhess-12-1693-2012*

Chen, H. K., Tang, H. M., & Chen, Y. I. (2006), Research on method to calculate velocities of solid phase and liquid phase in debris flow. *Applied Mathematics and Mechanics (English Edition)*, 27(3), 399-408. *https://doi.org/10.1007/s10483-006-0317-z*

Chen, H. X., Li, J., Feng, S. J., Gao, H. Y., & Zhang, D. M. (2019), Simulation of interactions between debris flow and check dams on three-dimensional terrain. *Engineering Geology*, 251, 48-62. *https://doi.org/10.1016/j.enggeo.2019.02.001*

590 Chen, T. Y. K., Hung, C. Y., Mullenbach, J., & Hill, K. (2022), Influence of fine particle content
591 in debris flows on alluvial fan morphology. *Scientific Reports*, 12(1), 21730.
592 https://doi.org/10.1038/s41598-022-24397-x
593 Chen, X. Q., Zhao, W. Y., & Gao, Q. (2011), Experimental investigation and design of artificial
594 structures controlling dam-break floods. *Journal of Southwest Jiaotong University*, 46(2),
595 228-234.
596 Cui, P., Zeng, C., & Lei, Y. (2015), Experimental analysis on the impact force of viscous debris
597 flow. *Earth Surface Processes and Landforms*, 40(12), 1644-1655.
598 https://doi.org/10.1002/esp.3744
599 Deng, Z., Li, Q., & Fu, H. (2008), Comparison between mechanical properties of dam and sieved
600 concretes. *Journal of materials in civil engineering*, 20(4), 321-326.
601 Dowling, C. A., & Santi, P. M. (2014), Debris flows and their toll on human life: a global
602 analysis of debris-flow fatalities from 1950 to 2011. *Natural hazards*, 71, 203-227.
603 https://doi.org/10.1007/S11069-013-0907-4
604 Gao, P.W., Lu, X.L., Lin, H., Li, X.Y., & Hou, J. (2007), Effects of fly ash on the properties of
605 environmentally friendly dam concrete. *Fuel*, 86(7-8), 1208-1211.
606 https://doi.org/10.1016/j.fuel.2006.09.032
607 Gao, Q., Chen, X.Q., Jia, S.T., & Huang, k. (2011), Experiment of Drainage Canal with
608 Indented-sill for Viscous Debris Flow. *Journal of Mountain Science*, 29 (1): 101–108. (in
609 Chinese) https://doi.org/10.16089/j.cnki.1008-2786.2011.01.014
610 Godt, J. W., & Coe, J. A. (2007), Alpine debris flows triggered by a 28 July 1999 thunderstorm
611 in the central Front Range, Colorado. *Geomorphology*, 84(1-2), 80-97.
612 https://doi.org/10.1016/j.geomorph.2006.07.009
613 Han, Z., Chen, G., Li, Y., Tang, C., Xu, L., He, Y., Huang, X., & Wang, W. (2015a), Numerical
614 simulation of debris-flow behavior incorporating a dynamic method for estimating the
615 entrainment. *Engineering geology*, 190, 52-64.
616 https://doi.org/10.1016/j.enggeo.2015.02.009
617 Han, Z., Chen, G., Li, Y., Wang, W., & Zhang, H.（2015b), Exploring the velocity distribution
618 of debris flows: an iteration algorithm based approach for complex cross-sections.
619 *Geomorphology*, 241, 72-82. https://doi.org/10.1016/j.geomorph.2015.03.043
620 Han, Z., Su, B., Li, Y., Wang, W., Wang, W., Huang, J., & Chen, G. (2019), Numerical
621 simulation of debris-flow behavior based on the SPH method incorporating the Herschel-
622 Bulkley-Papanastasiou rheology model. *Engineering Geology*, 255, 26-36.
623 https://doi.org/10.1016/j.enggeo.2019.04.013
624 Han, Z., Chen, G., Li, Y., Xu, L., Zheng, L., & Zhang, Y. (2014), A new approach for analyzing
625 the velocity distribution of debris flows at typical cross-sections. *Natural hazards*, 74,
626 2053-2070. https://doi.org/10.1007/s11069-014-1276-3
627 Han, Z., Yang, F., Li, Y., Dou, J., Chen, N., Hu, G., Chen, G.Q., & Xu, L. (2021), GIS-based
628 three-dimensional SPH simulation for the 11 april 2018 yabakei landslide at oita nakatsu,
629 Japan. *Water*, 13(21), 3012. https://doi.org/10.3390/W13213012
630 Hasanpour, A., Istrati, D., & Buckle, I. (2021), Coupled SPH–FEM modeling of tsunami-borne
631 large debris flow and impact on coastal structures. *Journal of Marine Science and*
632 *Engineering*, 9(10), 1068.
633 Horiguchi, T., & Richefeu, V. (2020), Post-analysis simulation of the collapse of an open sabo
634 dam of steel pipes subjected to boulder laden debris flow. *International Journal of*
635 *Sediment Research*, 35(6), 621-635. https://doi.org/10.1016/j.ijsrc.2020.05.002

636 Huang, G., Lv, G., Zhang, S., Huang, D., Zhao, L., Ni, X., Liu, H.W., Lv, J.H., & Liu, C. (2022),
637 Numerical analysis of debris flows along the Sichuan-Tibet railway based on an
638 improved 3D sphere DDA model and UAV-based photogrammetry. *Engineering*
639 *Geology*, 305, 106722. https://doi.org/10.1016/J.ENGGEO.2022.106722
640 Huang, Y., & Dai, Z. (2014), Large deformation and failure simulations for geo-disasters using
641 smoothed particle hydrodynamics method. *Engineering Geology*, 168, 86-97.
642 https://doi.org/10.1016/j.enggeo.2013.10.022
643 Huang, Y., Zhang, W., Xu, Q., Xie, P., & Hao, L. (2012), Run-out analysis of flow-like
644 landslides triggered by the Ms 8.0 2008 Wenchuan earthquake using smoothed particle
645 hydrodynamics. *Landslides*, 9, 275-283. https://doi.org/10.1007/s10346-011-0285-5
646 Huang, Y., & Zhu, C. (2015), Numerical analysis of tsunami–structure interaction using a
647 modified MPS method. *Natural Hazards*, 75, 2847-2862. https://doi.org/10.1007/s11069-
648 014-1464-1
649 Hungr, O., & McDougall, S. (2009), Two numerical models for landslide dynamic analysis.
650 *Computers & geosciences*, 35(5), 978-992. https://doi.org/10.1016/j.cageo.2007.12.003
651 Hübl, J., Suda, J., Proske, D., Kaitna, R., & Scheidl, C. (2009), Debris flow impact estimation. *In*
652 *Proceedings of the 11th international symposium on water management and hydraulic*
653 *engineering,* Ohrid, Macedonia, pp. 1-5.
654 Ishikawa, N., Shima, J., Matsuzawa, R., & Mizuyama, T. (2018), Safety verification of Sabo
655 dams against large scale debris flow. *In Symposium Proceedings of the*
656 *INTERPRAEVENT in the Pacific Rim*, Nara, Toyama, Japan, pp. 1-4.
657 Jia, S. T., Cui, P., Chen, X. Q., Huang, K., & Li, Q. (2011), Experimental study of regulating
658 barrage and transportation properties of debris flow by silt-trap dam. *Chinese Journal of*
659 *Rock Mechanics and Engineering*, 30(11), 2338-2345. (in Chinese)
660 Lian, Y., Bui, H. H., Nguyen, G. D., Tran, H. T., & Haque, A. (2021), A general SPH framework
661 for transient seepage flows through unsaturated porous media considering anisotropic
662 diffusion. *Computer Methods in Applied Mechanics and Engineering*, 387, 114169.
663 https://doi.org/10.1016/j.cma.2021.114169
664 Liang, S., & Chen, Z. (2019), SPH-FEM coupled simulation of SSI for conducting seismic
665 analysis on a rectangular underground structure. *Bulletin of Earthquake Engineering*, 17,
666 159-180. https://doi.org/10.1007/s10518-018-0456-z
667 Liang, W., & Zhao, J. (2019), Multiscale modeling of large deformation in geomechanics.
668 *International Journal for Numerical and Analytical Methods in Geomechanics*, 43(5),
669 1080-1114. https://doi.org/10.1002/nag.2921
670 Lichtenhahn, C. (1973), Berechnung von sperren in beton und eisenbeton. *Mitt Forstl Bundes*
671 *Versuchsanst Wein*, 102: 91–127. https://doi.org/10.3/JQUERY-UI.JS
672 Liu, D. C., You, Y., Du, J., Liu, J., Guan, J., & Liu, Y. (2019), Spatio-temporal distribution of
673 the impact force of debris flow. *Advanced Engineering Sciences*, 51(3), 17-25. (in
674 Chinese) https://doi.org/10.15961/j.jsuese.201801042
675 Iverson, R. M., Logan, M., LaHusen, R. G., & Berti, M. (2010), The perfect debris flow?
676 Aggregated results from 28 large-scale experiments. *Journal of Geophysical Research:*
677 *Earth Surface,* 115(F3). https://doi.org/10.1029/2009JF001514
678 Iverson, R. M., Reid, M. E., Logan, M., LaHusen, R. G., Godt, J. W., & Griswold, J. P. (2011),
679 Positive feedback and momentum growth during debris-flow entrainment of wet bed
680 sediment. *Nature Geoscience*, 4(2), 116-121. https://doi.org/10.1038/ngeo1040

McDougall, S., & Hungr, O. (2005), Dynamic modelling of entrainment in rapid landslides. *Canadian Geotechnical Journal*, 42(5), 1437-1448. https://doi.org/10.1139/t05-064

MIZUYAMA, T. (2008), Structural countermeasures for debris flow disasters. *International Journal of Erosion Control Engineering*, 1(2), 38-43. https://doi.org/10.13101/ijece.1.38

Moriguchi, S., Borja, R. I., Yashima, A., & Sawada, K. (2009), Estimating the impact force generated by granular flow on a rigid obstruction. *Acta Geotechnica*, 4, 57-71. https://doi.org/10.1007/s11440-009-0084-5

Morikawa, D. S., & Asai, M. (2022), A phase-change approach to landslide simulations: Coupling finite strain elastoplastic TLSPH with non-Newtonian IISPH. *Computers and Geotechnics*, 148, 104815. https://doi.org/10.1016/J.COMPGEO.2022.104815

Schaefer, L. N., Santi, P. M., & Duron, T. C. (2021), Debris flow behavior during the September 2013 rainstorm event in the Colorado Front Range, USA. *Landslides*, 18, 1585-1595. https://doi.org/10.1007/s10346-020-01590-5

Shieh, C. L., Ting, C.H., & Pan, H.W., (2008), Impulsive force of debris flow on a curved dam. International journal of sediment research, 23(2), 149-158. https://doi.org/10.1016/S1001-6279(08)60014-1

Song, D., Ng, C. W. W., Choi, C. E., Zhou, G. G., Kwan, J. S., Koo, & R. C. H. (2017), Influence of debris flow solid fraction on rigid barrier impact. *Canadian geotechnical journal*, 54(10), 1421-1434. https://doi.org/10.1139/cgj-2016-0502

Stoffel, M., Tiranti, D., & Huggel, C. (2014), Climate change impacts on mass movements—case studies from the European Alps. *Science of the Total Environment*, 493, 1255-1266. https://doi.org/10.1016/j.scitotenv.2014.02.102

Tang, C., Rengers, N. V., Van Asch, T. W., Yang, Y. H., & Wang, G. F. (2011), Triggering conditions and depositional characteristics of a disastrous debris flow event in Zhouqu city, Gansu Province, northwestern China. *Natural Hazards and Earth System Sciences*, 11(11), 2903-2912. https://doi.org/10.5194/nhess-11-2903-2011

Tiberghien, D., Laigle, D., Naaim, M., Thibert, E., & Ousset, F. (2007), Experimental investigations of interaction between mudflow and an obstacle. *In: Debris-flow hazards mitigation: mechanics, prediction and assessment*, Millpress, Rotterdam, 681-687.

Tsuguti, H., Seino, N., Kawase, H., Imada, Y., Nakaegawa, T., & Takayabu, I. (2019), Meteorological overview and mesoscale characteristics of the Heavy Rain Event of July 2018 in Japan. Landslides, 16, 363-371. https://doi.org/10.1007/s10346-018-1098-6

Wang, H., Wang, L., Song, Y., & Wang, J. (2016), Influence of free water on dynamic behavior of dam concrete under biaxial compression. *Construction and Building Materials*, 112, 222-231. https://doi.org/10.1016/j.conbuildmat.2016.02.090

Wang, X.L., Li, J.L., & Ma, X.T. (2015), Analysis on impact resistance performance of a new type of debris flow dam with braces based on CFX-ANSYS fluid-structure interaction. Journal of Safety and Environment, 15 (6): 101–105. (in Chinese). https://doi.org/10.13637/j.issn.1009-6094.2015.06.020

Wang, Z.C., & Li, D.M. (2017), Fluid-structure coupling algorithm based on SPH-DEM and application to simulate landslide surge. *Yantu Lixue/Rock and Soil Mechanics*, 38 (4). (in Chinese). https://doi.org/10.16285/j.rsm.2017.04.038

Yan, H., Wang, Z., He, J., Chen, X., Wang, C., & Peng, Q. (2009), Real-time fluid simulation with adaptive SPH. *Computer Animation and Virtual Worlds*, 20(2-3), 417-426. https://doi.org/10.1002/cav.300

726 Yu, D., Tang, L., & Chen, C. (2020), Three-dimensional numerical simulation of mud flow from
727 a tailing dam failure across complex terrain. *Natural Hazards and Earth System Sciences*,
728 20(3), 727-741. https://doi.org/10.5194/nhess-20-727-2020
729 Yu, X., Chen, X., Wang, H., & Jia, C. (2020), Numerical study on the interaction between debris
730 flow slurry and check dams based on fluid–solid coupling theory. *Geotechnical and*
731 *Geological Engineering*, 38, 2427-2445. https://doi.org/10.1007/s10706-019-01160-0
732 Zhu, C., Chen, Z., & Huang, Y. (2021), Coupled moving particle simulation–finite-element
733 method analysis of fluid–structure interaction in geodisasters. *International Journal of*
734 *Geomechanics*, 21(6), 04021081.
735 Zhu, C., Huang, Y., & Zhan, L.T. (2018), SPH-based simulation of flow process of a landslide at
736 Hongao landfill in China. *Natural Hazards*, 93, 1113-1126.
737 https://doi.org/10.1007/s11069-018-3342-8